(TEMPOL). The data are the mean ± SD from 4 animals for each group. **(B)** Kinetics of the nitroxide-enhanced MRI signal in the brain before and after injection of oxidized nitroxide (TEMPOL). The data are the mean ± SD from 6 animals for the control group and 4 animals for all other groups. **(C)** Amplitude of the EPR signal in isolated tissue specimens after addition of reduced TEMPOL. The data are the mean ± SD from 4 animals for each group. *p<0.05; **p<0.01; ***p<0.001.

Figure 7. (A) Total antioxidant capacity (TAC) of brain tissue in healthy and neuroblastoma-bearing mice. The data are the mean ± SD from 4 animals for each group. In the control group, TAC was considered 100%, which corresponded to 12 μM uric acid equivalents per mg protein (~26 μM copper reducing equivalents per mg protein). **(B)** Plasma levels of matrix metalloproteinases (MMP2 and MMP9) in healthy and neuroblastoma-bearing mice. The data are the mean ± SD from 4 animals for each group; *p<0.05; **p<0.01; ***p<0.001.

Figure 8. Typical nitroxide-enhanced MR images of healthy and cancer-bearing mice in the early or terminal stage of cancer (brain neuroblastoma or brain glioma): (a) MR images of the brain with arrows indicating the tumor; (b, c) extracted nitroxide-enhanced MRI signal obtained 6 min and 14 min after injection of SLENU.

Figure 9. Molecular hypothesis.
The inoculation of cancer cells in the brain can be considered an "inflammatory signal." The inoculation leads to a local migration and an activation of immune cells in the microenvironment of the primary tumor locus. ROS/RNS, produced by the activated immune cells in the grafted area, could provoke signal transduction in three targets with equal probability: (i) grafted cancer cells, (ii) surrounding normal cells and (iii) the surrounding extracellular matrix.

ROS/RNS and cross-talk between cancer cells and the extracellular matrix activate the integrin signaling cascade. The oncogenic miRNAs, secreted by cancer cells into the environment, are considered a primary mediator of this process. The activation of integrins is linked to additional ROS/RNS production, leading to a vicious cycle. As a result, the tissue redox balance shifts toward oxidation.

Cancer cells are adapted to high levels of ROS/RNS and survive. However, the normal surrounding cells and extracellular matrix are not adapted to this abnormal free radical attack and can undergo irreversible changes.

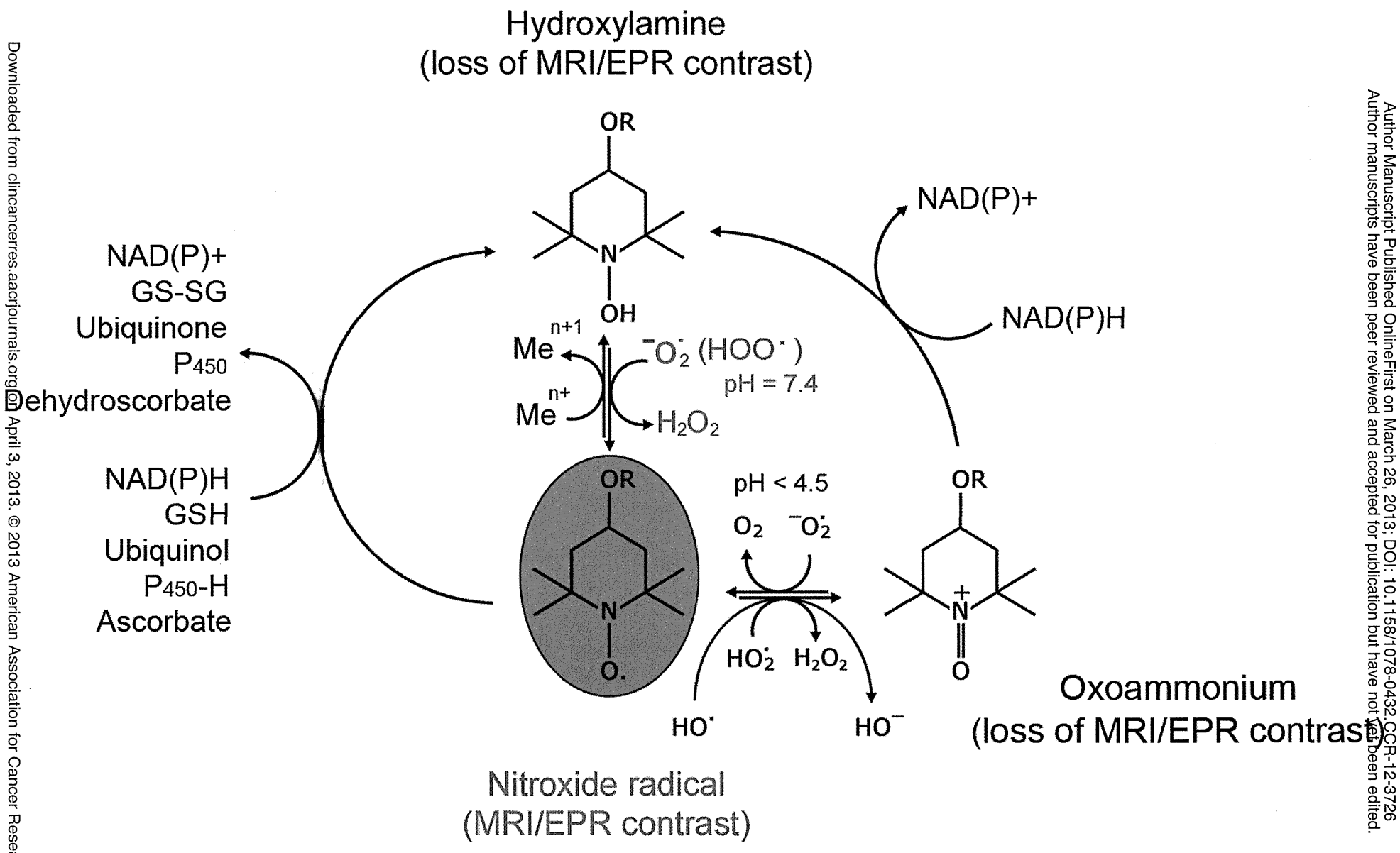

Figure 1

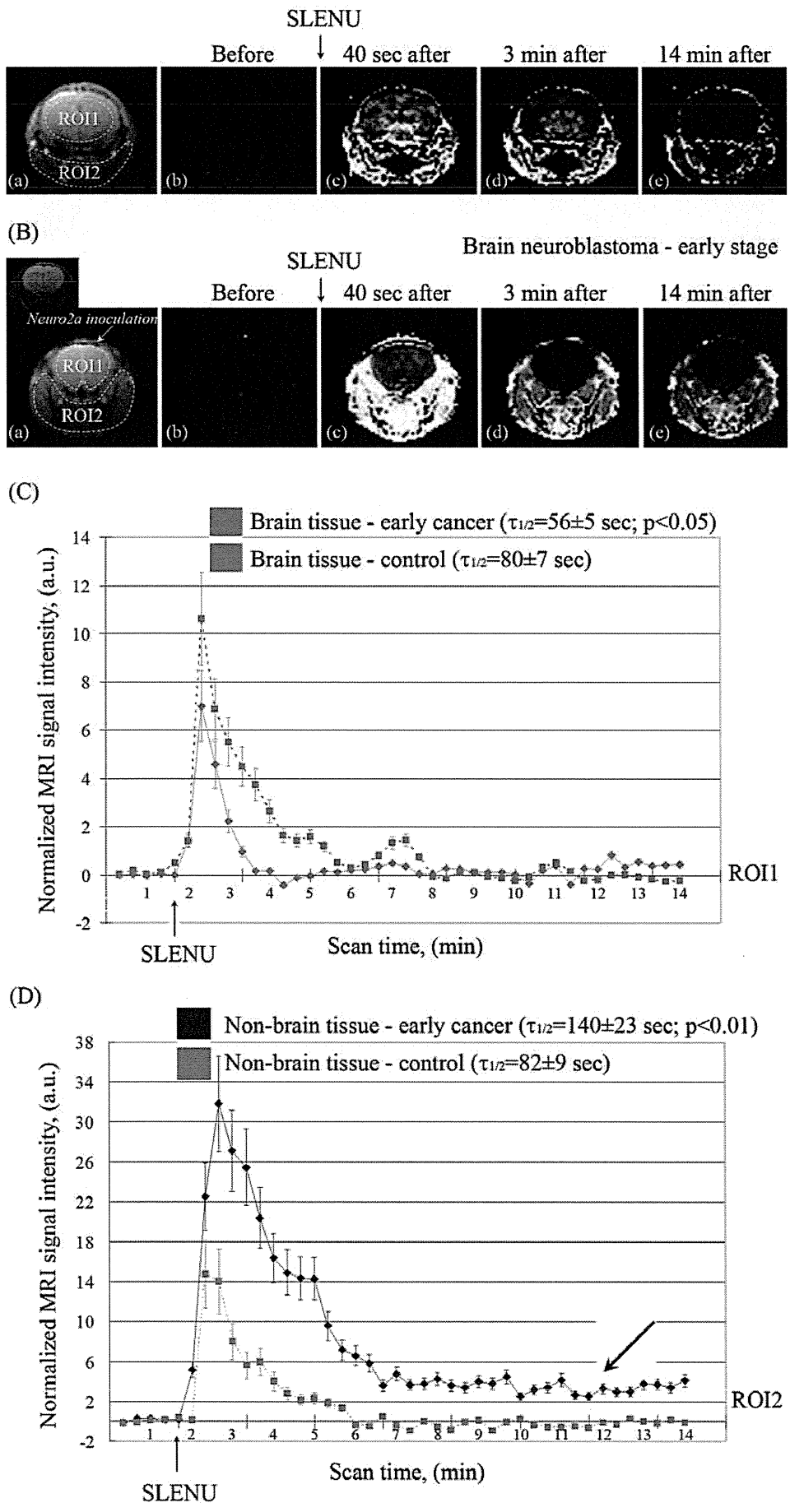

Figure 2

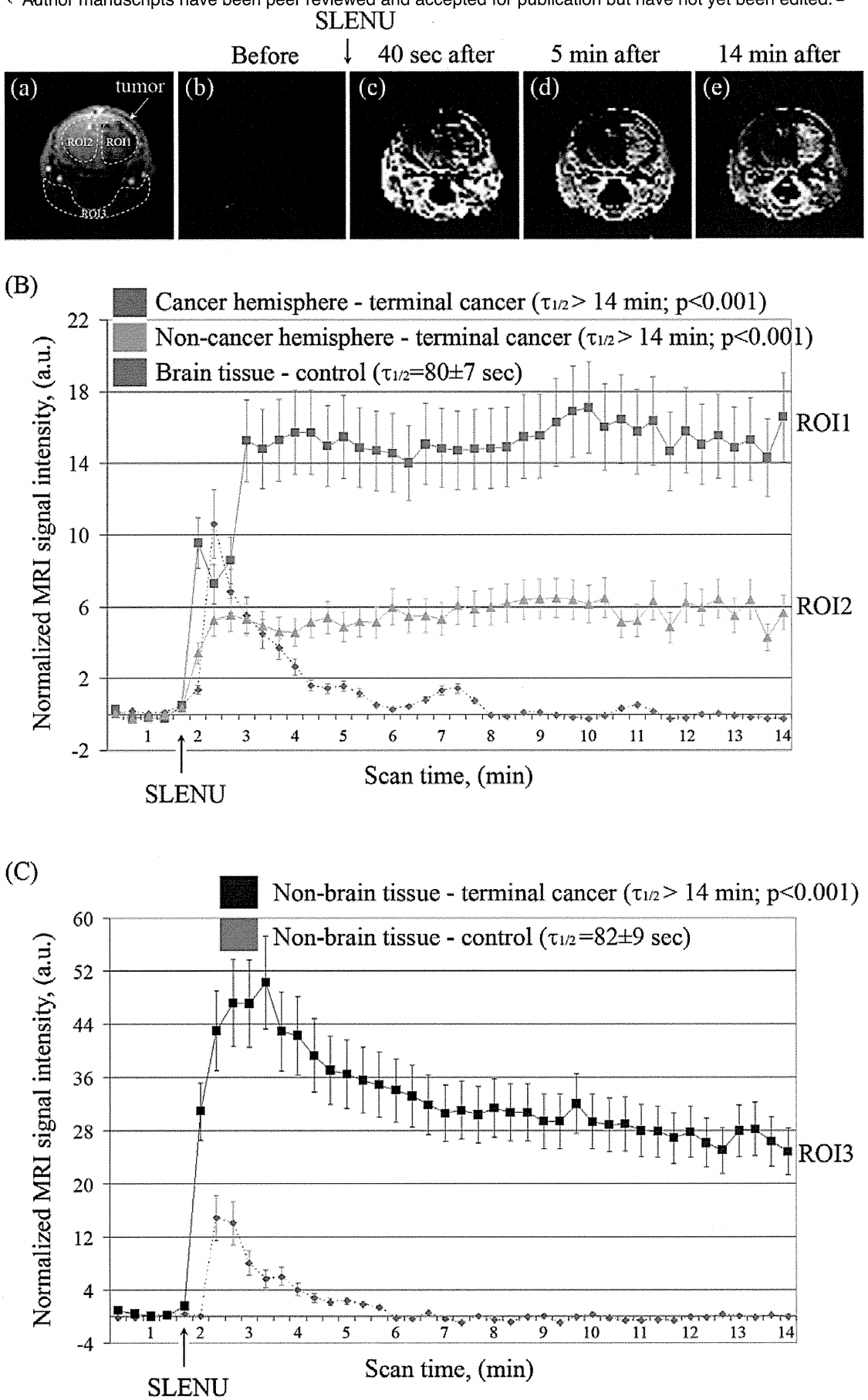

Figure 3

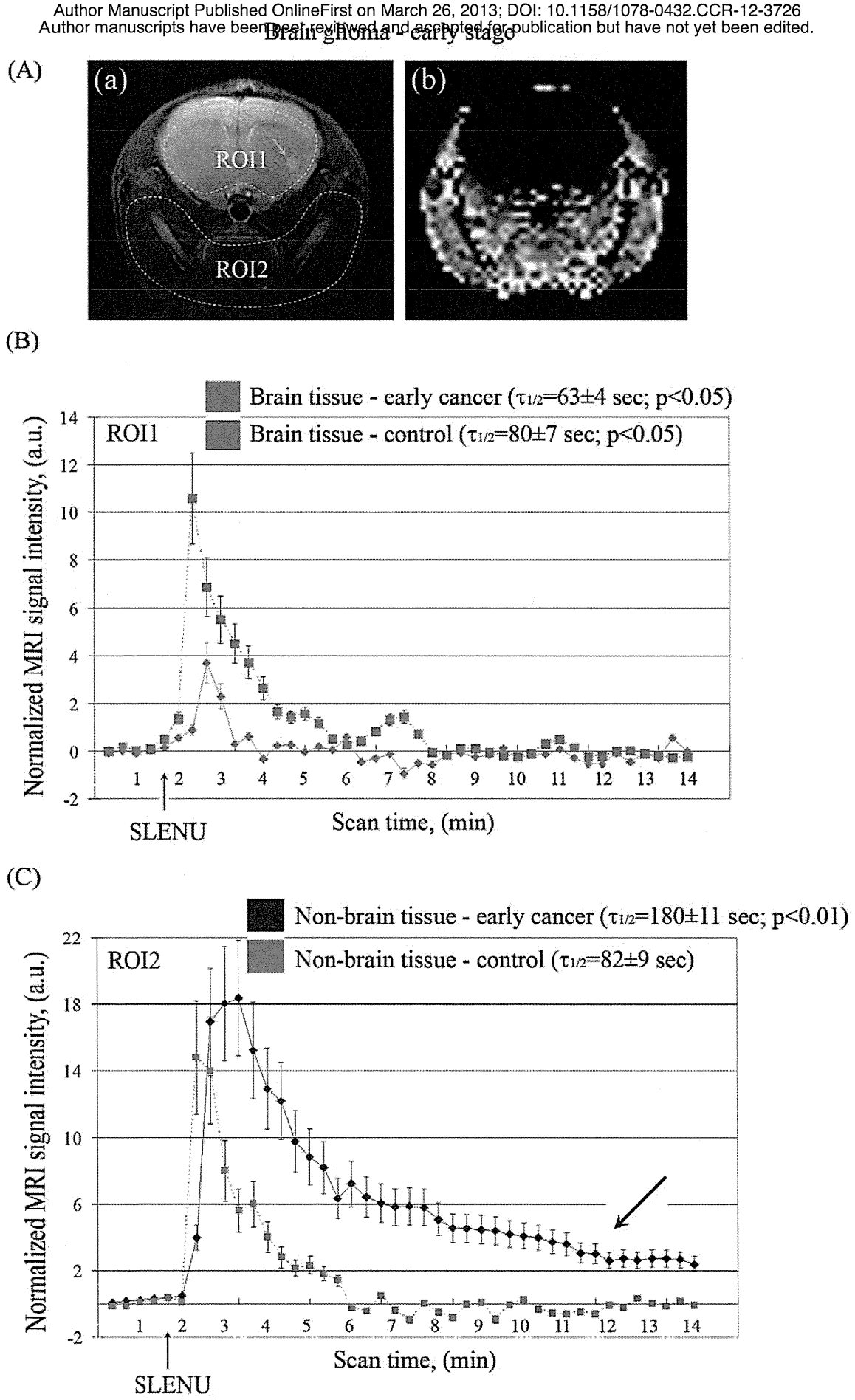

Figure 4

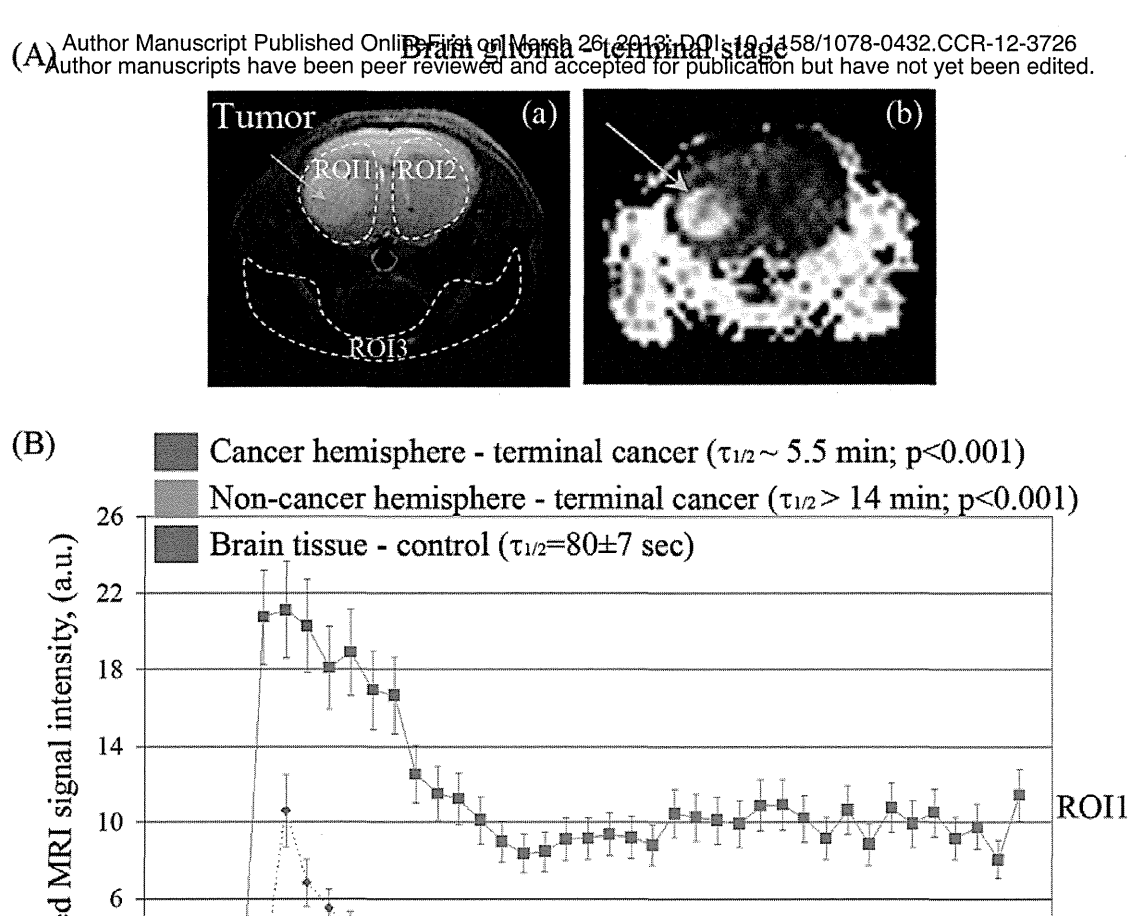

Figure 5

Figure 6

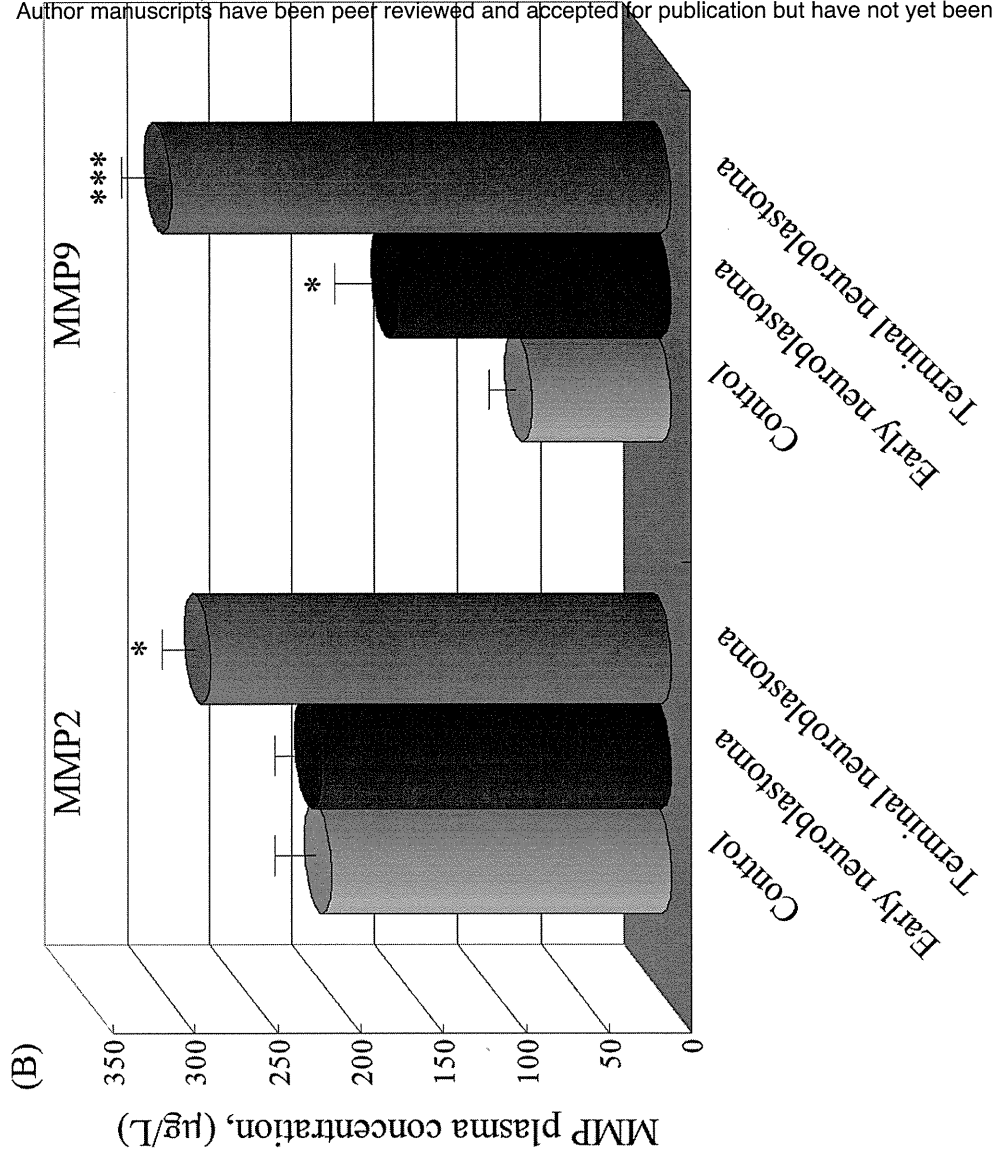

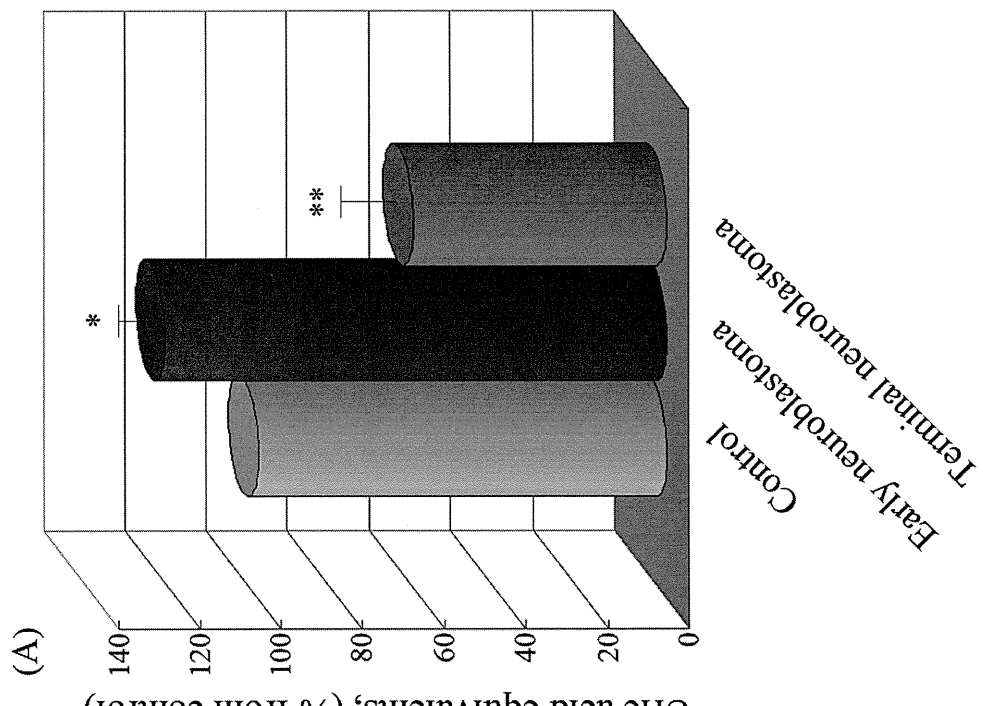

Figure 7

Figure

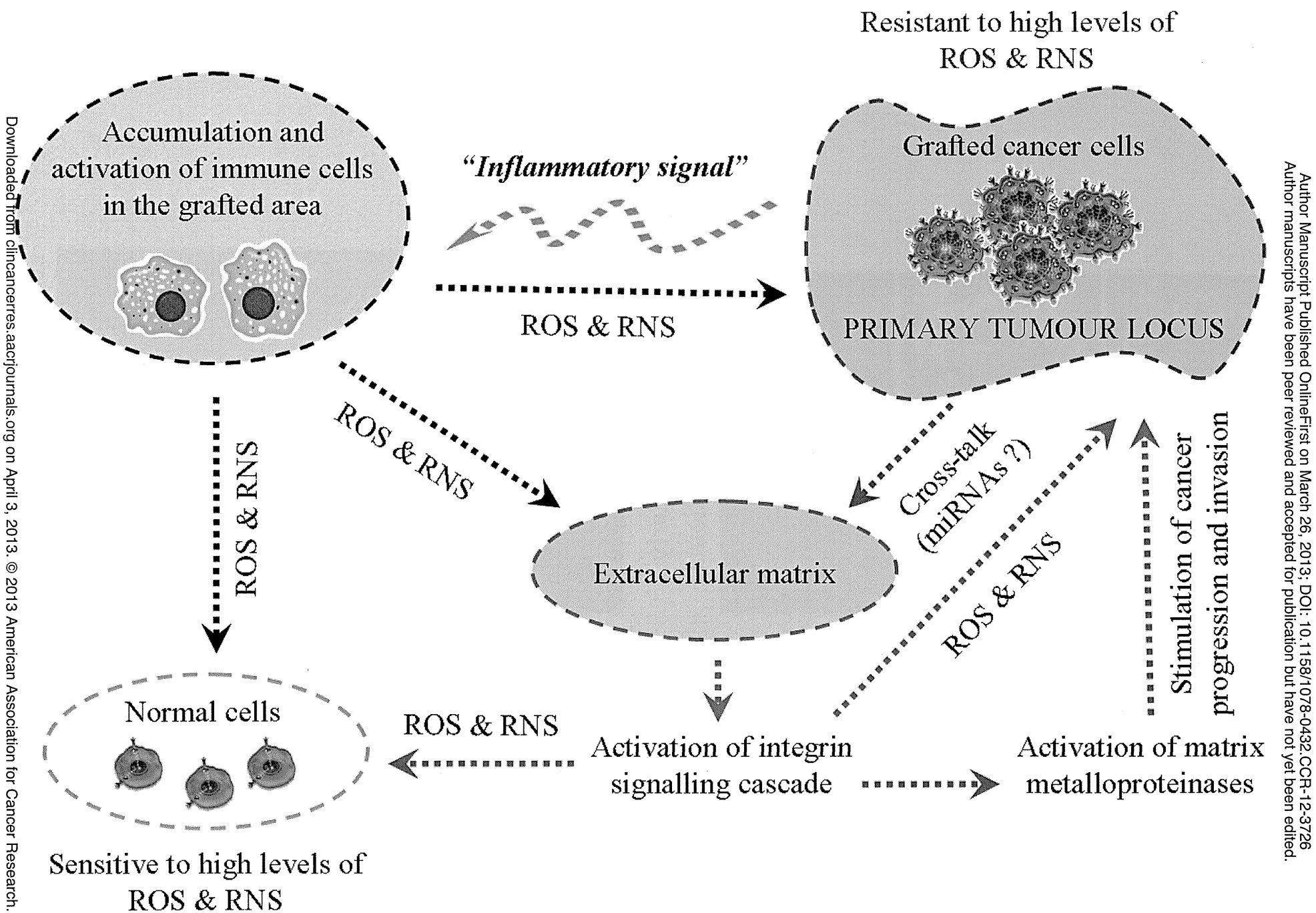

Figure 9

Original Research

In Vivo Identification of Sentinel Lymph Nodes Using MRI and Size-Controlled and Monodispersed Magnetite Nanoparticles

Shuji Iida, MD,[1] Kensuke Imai, MS,[2] Sachiko Matsuda, PhD,[1] Osamu Itano, MD, PhD,[1]* Mamoru Hatakeyama, PhD,[3] Satoshi Sakamoto, PhD,[2] Daisuke Kokuryo, PhD,[4] Koji Okabayashi, MD,[1] Takashi Endo, MD,[1] Yoshiyuki Ishii, MD, PhD,[1] Hirotoshi Hasegawa, MD, PhD,[1] Ichio Aoki, PhD,[4] Hiroshi Handa, MD, PhD,[2,3] and Yuko Kitagawa, MD, PhD[1]

Purpose: To develop a sentinel lymph node (SN) identification method using accurately synthesized magnetic nanoparticles (MNPs), as an enhanced specific SN tracer in combination with magnetic resonance imaging (MRI) in intact rodent and SN metastasis models.

Materials and Methods: Three sizes of MNPs were originally synthesized. We developed an experimental rat SN model, with brachial lymph nodes (Br) as the SN and the axillary lymph node (Ax) as the second lymph node, and injection of MNPs via the front paw. SN detectability was evaluated in vivo using T_1-weighted MR images after injection of the synthesized MNPs, and the amount of iron in the Br and in the Ax was assessed using inductively coupled plasma optical emission spectrometry.

Results: The highest ratios of the amount of iron in the Br versus the Ax were 3.1 and 3.3, using 20-nm MNPs after 2- and 24-hour injections. The appropriate dose and particle diameter for MRI detection was optimized, and the SN was optimally distinguished in the normal and metastatic rat models using MRI after a 0.4 mg/kg 20-nm MNP injection.

Conclusion: We developed and optimized a useful SN identification method using MRI in rodent models.

Key Words: magnetic nanoparticles; MRI; sentinel lymph node; detection
J. Magn. Reson. Imaging 2013; 000:000–000.

THE DETERMINATION OF THE SPREAD of metastatic cancer to lymph nodes (LNs) and the histopathological status of tumor draining regional LNs are significant predictors of recurrence and overall survival for most solid malignancies, and are often used to justify the stratification of patients for adjuvant therapy (1,2). The first LN that receives lymphatic drainage from a primary tumor is defined as a sentinel lymph node (SN), and when metastasis is not found in an SN, it almost certainly will not be present in more distal LNs. The primary benefit of SN mapping and biopsy is that it enables surgeons to avoid nontherapeutic LN dissection and the complications that can be caused. SN biopsy is currently used in various organs, such as the colon (3–5), esophagus (6,7), and gastrointestinal tract (6,8).

The ideal SN imaging agent needs to travel quickly through the lymphatic channels and be retained in the SN for a significant period of time. Currently there are no imaging agents that can be used both preoperatively and intraoperatively with a single injection. The techniques used to detect the SN during surgery have focused on the use of a vital blue dye (9), a radioactive tracer (10), or a combination of both (11). In the clinic, dye and radioactive tracer techniques have some problems associated with their use, such as anaphylactic shock, difficulties in detection, exposure to radiation, and limitations connected with the use of radioisotopes (12,13). Additionally, there is no useful method for preoperative SN screening of the whole body, with the exception of radioscintigraphy, which has relatively poor spatial resolution. Ultrasmall superparamagnetic iron oxide (USPIO) particles have been introduced as a contrast agent for magnetic

[1]Department of Surgery, School of Medicine, Keio University, Tokyo, Japan.
[2]Department of Biological Information, Graduate School of Bioscience and Biotechnology, Tokyo Institute of Technology, Yokohama, Japan.
[3]Solutions Research Laboratory, Tokyo Institute of Technology, Yokohama, Japan.
[4]Molecular Imaging Center, National Institute of Radiological Sciences (NIRS), Japan.
Contract grant sponsor: Special Coordination Funds for Promoting Science and Technology from the Japan Science and Technology Agency; Contract grant sponsor: Kakenhi (JSPS); Contract grant sponsor: Funding Program for World-Leading Innovative R&D on Science and Technology (FIRST Program).
*Address reprint requests to: O.I., Department of Surgery, School of Medicine, Keio University, 35 Shinanomachi, Shinjuku-ku, Tokyo 160-8582, Japan. E-mail: laplivertiger@gmail.com
Received September 9, 2012; Accepted February 11, 2013.
DOI 10.1002/jmri.24108
View this article online at wileyonlinelibrary.com.

resonance imaging (MRI) (14–16). Studies of patients with head and neck, urologic, pelvic, gastric, esophageal, and breast cancers have confirmed the improved detection of LN metastases with USPIO-enhanced MRI (14,17–22), but it remains difficult to identify the SN. USPIO particles are not suitable for SN identification because they can track beyond the first node and into the second echelon nodes.

SN localization of tracer is influenced by several factors that include method and site of injection, dose, and particle size. Of these, particle size is one of the most important, but there is no agreement concerning the optimal particle size of the ideal colloid.

To overcome these problems, new magnetic nanoparticles (MNPs) were developed as a specific tracer for SNs (23). To improve the specificity of SN targeting, our MNPs had two special features: size and stable dispersion in solution owing to the manufactured surface coating. The purpose of the present study was to evaluate if the improved MNPs can work as an SN-specific tracer and have sufficient detectability for SN identification using MRI.

MATERIALS AND METHODS

Animal Preparation

All animal protocols were approved by the animal research committees. Male Donryu rats (Sankyo Labo Service, Tokyo, Japan) aged 5 weeks and weighing 230 ± 8 g were used for the optimization of MNP size ($n = 8$) and the amount injected ($n = 8$). For SN detection by MRI, 5-week-old male Donryu rats (Japan SLC, Shizuoka, Japan) weighing 198.0 ± 2.5 g were used ($n = 9$). Two male F344/NJcl-rnu/rnu nude rats (CLEA Japan, Tokyo, Japan) aged 4 weeks and weighing 193 ± 16 g were used for the establishment of the metastatic model, and seven of these rats weighing 172.0 ± 6.9 g were used for SN detection by MRI. For toxicity evaluation, two 6-week-old female BALB/c mice (Oriental Yeast, Tokyo, Japan) were used for the high-dose group and four for the low-dose group. Animals were maintained on a standard laboratory chow diet and had access to tap water ad libitum. During the entire procedures, anesthesia was induced and maintained in rats by means of 4% isoflurane inhalational (Mylan, Tokyo, Japan), and they were then ventilated with 1.5% isoflurane and a 1:2 O_2/room air gas mixture using a mechanical carburetor. Ferucarbotran as a control was injected into the forepaws at the same iron concentration as that of the MNPs.

Cell Lines

Human epithelial carcinoma cell line A431 (American Tissue Culture Collection, Rockville, MD [ATCC]) was used for stable transfection with green fluorescent protein (GFP). A431 cells were maintained in Dulbecco's modified Eagle's medium (DMEM) with 10% heat-inactivated fetal bovine serum (Gibco, Grand Island, NY) in a 5% (v/v) CO_2 humidified incubator at 37°C.

Rat Sentinel Metastatic Model

To establish the metastatic model, 2×10^6 A431 cells that stably expressed GFP (1×10^7 cells/mL in phosphate-buffered saline [PBS]) were injected into the forepaw of 4-week-old male nude rats. LNs were extracted after 18 days of implantation, and metastasis was visualized under a fluorescence stereoscopic microscope.

Magnetite Nanoparticle Preparation

Three MNPs whose particle sizes were 4, 8, and 20 nm (abbreviated M4, M8, and M20, respectively) were prepared according to previous reports (23–25). Since the three MNPs were citrate-coated magnetite nanoparticles based on reported highly size-controlled nanocrystals (21), they are monodispersed in water. A conventional contrast agent, Ferucarbotran (Resovist, Fujifilm Pharma, Tokyo, Japan), was used as a control. Ferucarbotran is an MRI contrast agent that is a hydrophilic colloid composed of carboxydextran-coated iron oxide nanoparticles comprising multiple crystals. The overall hydrodynamic diameter of Ferucarbotran was 62.3 ± 18.7 nm measured using dynamic light scattering (FPAR-1000, Otsuka Electronics, Osaka, Japan).

Surgical and Histological Procedures

A skin incision was performed over the popliteal fossa after an enhancing agent was injected into the front paw using a microsyringe with a 27G needle, and these spaces were explored for lymphatic channels or LNs. At the completion of popliteal fossa exploration, samples of tissue were harvested from the brachial lymph nodes (Br) and the axillary lymph node (Ax) and were subsequently pathologically evaluated. Harvested LN tissues were fixed in 10% neutral buffered formaldehyde and were processed for paraffin embedding. Microsections (4 μm) were prepared with a microtome and were deparaffinized in xylol. They were then rehydrated in a descending ethanol series and stained with Prussian blue to detect iron particles in the cells.

Measurement of Magnetite in LNs

After injection of the agent, the Br and the Ax were harvested, weighed, and lyophilized. The lyophilized samples were dissolved in nitric acid. The amount of magnetite in the LNs was measured using inductively coupled plasma optical emission spectrometry (ICP-OES) (Perkin Elmer Optima 3000 XL ICP-OES Spectrometer, Kanagawa, Japan).

MRI

To examine whether or not the SN could be detected using MNPs in normal rats, and to determine if they could trace SNs with metastases in the metastatic rat model, they were injected into both forepaws. All MR images were acquired on a 7.0 T animal MRI (Magnet:

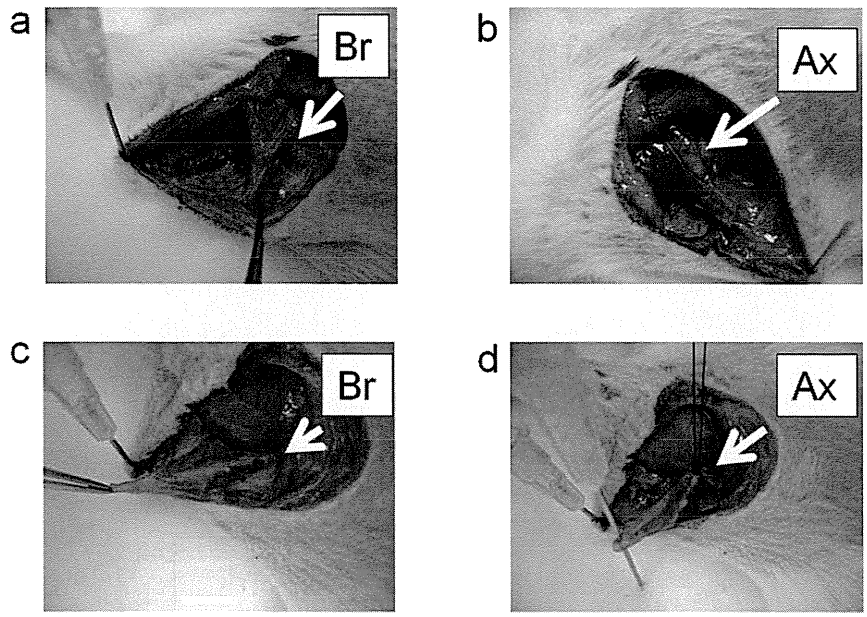

Figure 1. The brachial lymph node (Br) (**a**) and the axillary lymph node (Ax) (**b**) are shown. The lymphatic anatomy in the hind limb of the rat has been exposed to show the blue contiguously linked Br (**c**) and Ax (**d**) after injection of isosulfan blue into the front paw.

Kobelco, Kobe, Japan and JASTEC, Kobe, Japan; Console: Bruker Biospin, Ettlingen, Germany) with a 72-mm inner-diameter birdcage coil. Rats were initially anesthetized with 4.0% isoflurane (Mylan), orally intubated, and then ventilated with 1.5% isoflurane and a 1:2 O_2/room air gas mixture using a rodent ventilator (MRI-1: CWE, Ardmore, PA). Breaths per minute were set within a limit of 60–80. MRI scans were performed before and at 30 minutes after MNP injection. To avoid too strong a susceptibility effect in the MNPs, T_1-weighted contrast was employed using incoherent 2D gradient echo sequences (fast low-angle shot, FLASH) with fat suppression preparation pulse and respiratory gating. The parameters were as follows: TR/TE = 350–980/10 msec depending on respiratory gating; flip angle = 45°; slice thickness = 1.0 mm; slice gap = 0.5 mm; field of view = 60 × 60 mm^2; matrix = 256 × 256; number of slices = 13; and number of acquisitions = 4.

Exploratory MNP Single Toxicity Study

Mice were divided into five groups, and 20-nm MNPs were injected into the tail vein (control: saccharose fluid injection; low dose: 625 μmol/kg; medium-low dose: 1250 μmol/kg; medium-high dose: 2500 μmol/kg; and high dose: 5000 μmol/kg), which are the same doses as those tested in the toxicity study for Ferucarbotran according to the accompanying documentation from the manufacturer. Overall animal condition and weight changes were evaluated. Tissue samples of lung, liver, and spleen were examined histopathologically on postoperative day 7.

Data Analysis and Statistics

MR image analysis was performed using the MRVision image display and processing package (MRVision, Winchester, MA). Signal changes of LNs induced by MNPs were evaluated on MR images by two independent researchers. The negatively enhanced area (mm^2) in LNs was calculated by means of the ROI tool of the MRVision software. All results were expressed as the mean ± standard error. Statistical significance was determined using the Mann–Whitney *U*-test for MRI analysis. $P < 0.05$ was considered being statistically significant. In addition, all receiver operating characteristic (ROC) curve analyses of MRIs were carried out using the data from the negatively enhanced area. ROCs displaying sensitivity together with the false-positive rate (1-specificity) for detecting MNPs by MRI,

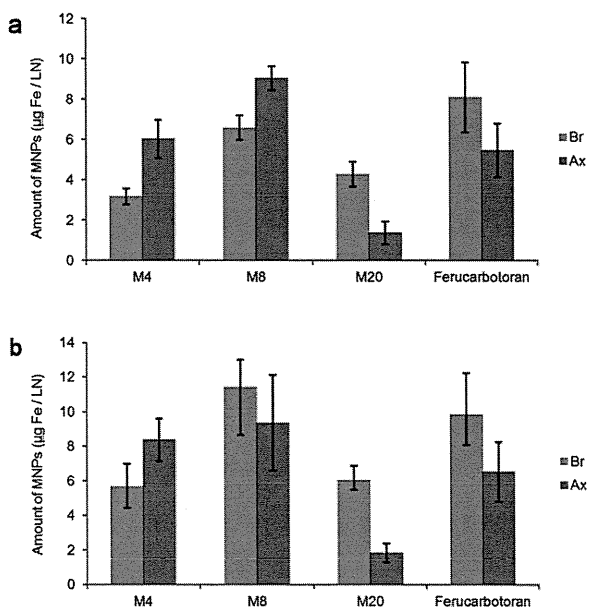

Figure 2. The amount of the three sizes of MNPs (M4, M8, and M20) and Ferucarbotran in the Br and Ax at 2 hours (**a**) and 24 hours (**b**) after injection.

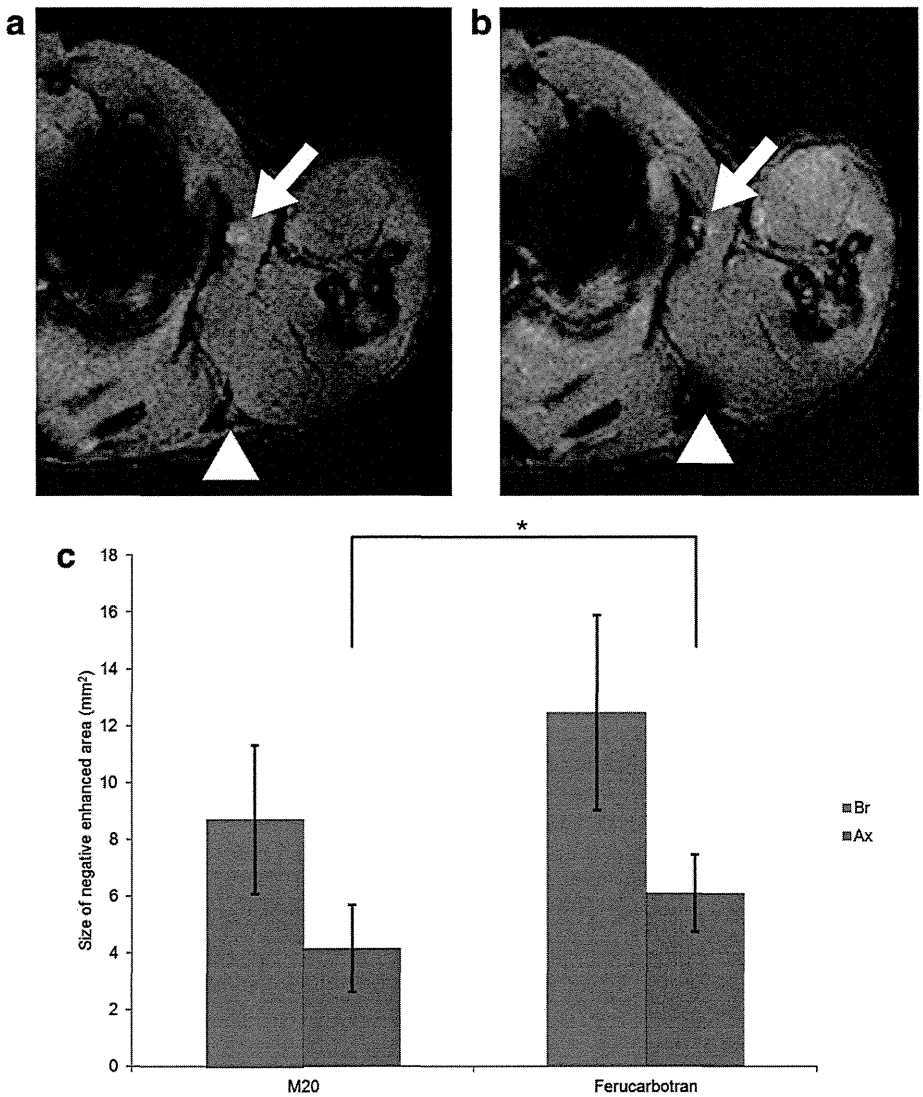

Figure 3. T_1-weighted gradient echo images obtained before (**a**) and after (**b**) magnetite administration in wildtype rats. The arrowhead indicates the Br and the arrow indicates the Ax. The sizes of the negative enhanced areas associated with M20-MNPs and Ferucarbotran nanoparticles are shown in (**c**).

and the area under the curve with 95% confidence intervals (CIs) were calculated. All statistical analyses were performed using Stat View v. 5.0 statistical software package (SAS Institute, Cary, NC).

RESULTS

Establishment of a Rat Model for SN Identification: Surgical Exposure

The Br in rats most often existed as three similarly sized (2–3 mm) nodes (Fig. 1a) and the Ax typically consisted of four to five nodes of 1–3 mm in size (Fig. 1b). To determine the SN of rats, the popliteal fossa was explored visually for any blue-colored lymphatic channels or LN within 3–5 minutes of injection of isosulfan blue into the front paw. The lymphatic anatomy in the hind limb of the rat was exposed to show blue contiguously linked Br (Fig. 1c) and Ax (Fig. 1d). The Br should represent the SN and the Ax should be a higher echelon node further downstream from the SN.

Determination of the Appropriate Diameter of MNPs as a Tracer for SN Identification

To investigate which was the most suitable diameter for a tracer, we measured and compared the levels of our MNPs (M4, M8, and M20) and Ferucarbotran in the Br and Ax at 2 hours (Fig. 2a) and 24 hours (Fig. 2b) after their injection by means of ICP-OES. For the initial experiment the dose of MNPs administered was 0.4 mg/kg according to the preliminary experiment. M20 was sustained in the SN and very little reached distant LNs even at 24 hours after injection. Conversely, M4, M8, and Ferucarbotran reached the Ax even after 2 hours. The ratio of the level of MNPs in the Br to the level of MNPs in the Ax was 3.1 after 2 hours and 3.3 after 24 hours using M20; this ratio

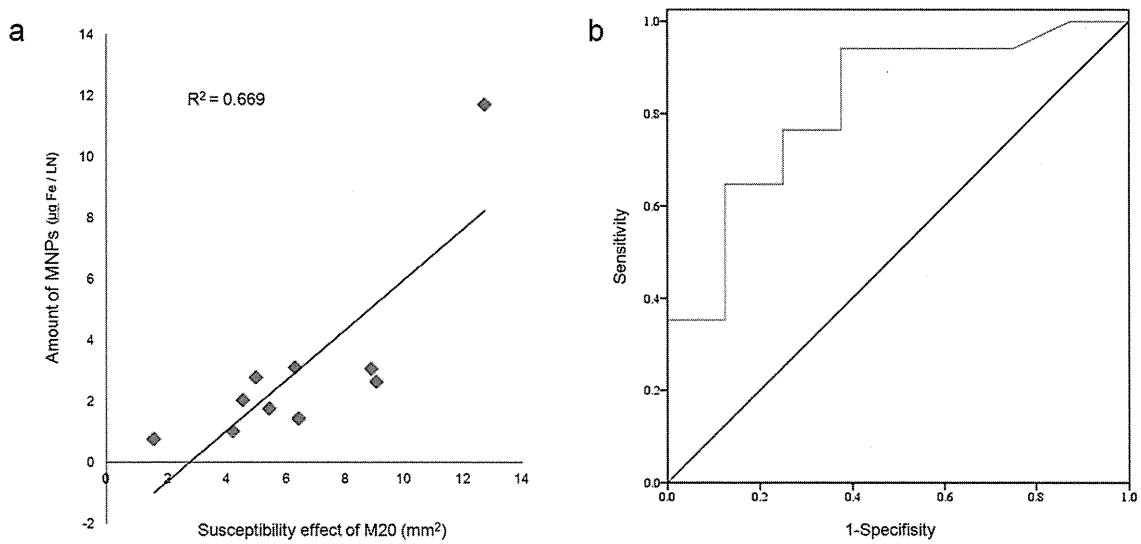

Figure 4. The optimal level of magnetite in the LN for MRI detection was evaluated. The relationship between the level of M20 in the LN and negatively enhanced area in the MR imaging is shown in direct proportion (R^2 = 0.669) (**a**). ROC curve analysis revealed that the threshold of the amount of magnetite required for MRI detection was 2.3 μg/LN (0.08 μg/mg tissue) with 76.5% sensitivity and 25% specificity, and the area under the ROC curve was 0.82 (95% CI, 0.64–1.0) (**b**).

was 0.5, 0.7, and 1.5 for M4, M8, and Ferucarbotran, respectively, after 2 hours, and 0.7, 1.2, and 1.5, respectively, after 24 hours. M20 had the highest ratio among these agents. This implied that M20 was the appropriate diameter for optimal identification of the SN in the SN models.

Determination of the Appropriate Amount of MNPs

Typical MR images are shown before (Fig. 3a) and after the injection of M20-MNPs (Fig. 3b). The influence of MNPs was evaluated in terms of the negatively enhanced area (mm^2) in MR images. In these images, clear signal reduction with a large susceptibility effect in the Br was observed after MNP injection, and there were no large alterations in the Ax. The average size of the negatively enhanced areas in the Ax measured using M20-MNPs (n = 5) was significantly smaller than those measured using Ferucarbotran (n = 4) (Fig. 3c). The results were mostly in agreement with the trend in the ICP-OEM results (Fig. 2). To determine the optimum level of magnetite in the LN for MRI detection, the relationship between the level of M20 in the LN and negatively enhanced area was evaluated. The relationship was in direct proportion as shown in Fig. 4a (R^2 = 0.669). In addition, analyses of the sensitivity and specificity of MRI detection were carried out. ROC curve analysis revealed that the threshold of the amount of magnetite required for MRI detection was 2.3 μg/LN (0.08 μg/mg tissue)

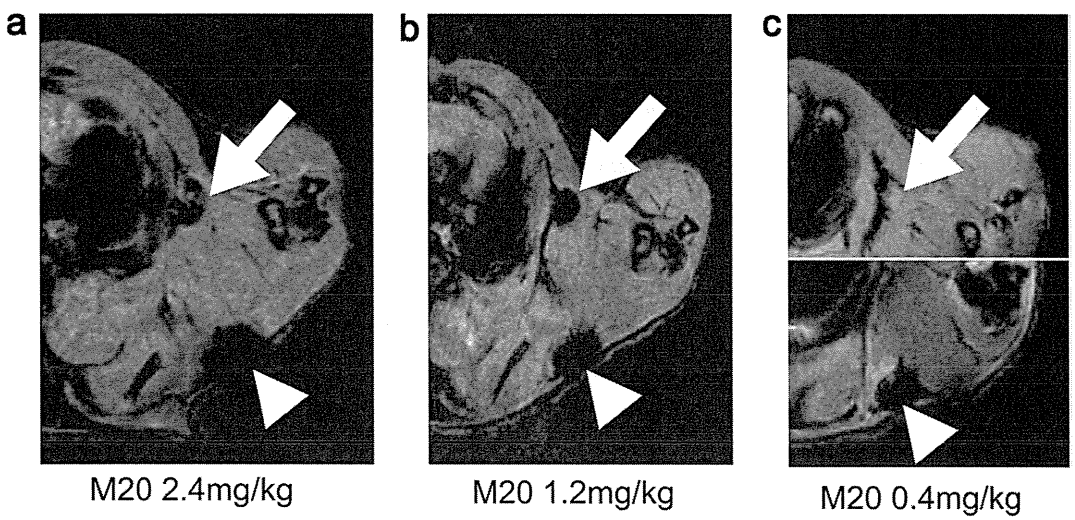

Figure 5. Comparison of the intensity level of the gradient echo image after 2.4 mg/kg (**a**), 1.2 mg/kg (**b**), and 0.4 mg/kg (**c**) injections of MNPs. The arrowhead indicates the Br and the arrow indicates the Ax.

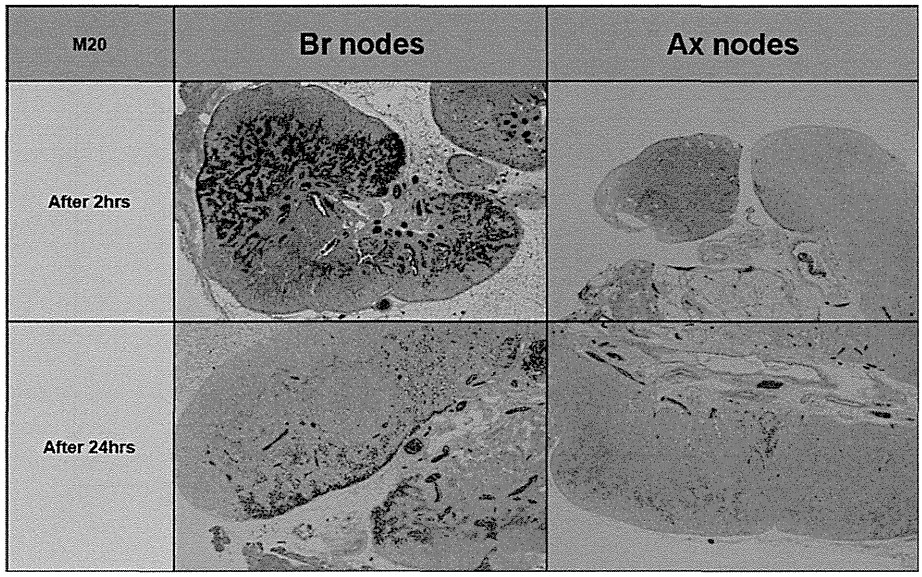

Figure 6. M20 MNPs in the Br and the Ax. The MNPs were injected into the rat front paw and the nodes were harvested after 2 and 24 hours. MNPs are colored blue owing to Prussian blue staining.

with 76.5% sensitivity and 25% specificity, and the area under the ROC curve was 0.82 (95% CI, 0.64–1.0) (Fig. 4b). The size of the signal reduction area evaluated may have been slightly larger than actual size because of the susceptibility effect, but detectability was improved.

Four different doses of M20 (2.4, 1.2, 0.4, and 0.2 mg/kg) were injected into the rat forepaw to find the optimal amount of MNPs for administration. In the case of M20 doses of 2.4 mg/kg and 1.2 mg/kg, signal intensity in both the Br and the Ax was decreased (Fig. 5a,b). The levels of MNPs in the Br and the Ax were 19.5 μg/Br (0.84 μg/mg tissue) and 3.2 μg/Ax (0.1 μg/mg tissue), respectively, in the case of the 2.4 mg/kg injection and 10.0 μg/Br (0.43 μg/mg) and 3.8 μg/Ax (0.12 μg/mg tissue), respectively, in the case of the 1.2 mg/kg injection. The level of MNPs in the Ax was higher than the threshold level 2.3 μg/LN (0.08 μg/mg tissue) for both the 2.4 mg/kg and 1.2 mg/kg injections, which indicated that not only the Br but also the Ax was detected by MRI. On the other hand, the signal intensity of the Br was decreased but that of the Ax did not change after a 0.4 mg/kg MNP injection (Fig. 5c). The level of MNPs in the Br was 0.94 μg/LN (0.04 μg/mg tissue) after a 0.2 mg/kg injection, and this was under the threshold. This implied that 0.4 mg/kg was the appropriate dose of injected magnetite to identify the SN in the case of M20 using rat SN models.

Pathological Evaluation

To confirm whether MNPs were retained in the Br after administration, the LN was evaluated pathologically using Prussian blue staining at 2 and 24 hours after injection of 0.4 mg/kg M20 (Fig. 6). MNPs were predominantly retained in the Br with very little in the Ax at both 2 and 24 hours. These results were consistent with the results described above. They confirmed that M20 was the MNP with appropriate diameter for SN identification and that 0.4 mg/kg was the optimal dose for injection.

Establishment of the Metastatic Rat Model and SN Identification Using MRI

At 18 days after the injection of A431 cells the Br and the Ax were harvested for evaluation. Fluorescent stereoscopic microscopy revealed metastatic tumor (Fig. 7a,b), and this was confirmed histologically with hematoxylin and eosin (H&E) staining (Fig. 7c) and a fluorescence microscope (Fig. 7d). Metastatic tumors were only seen in the Br and not in the Ax (data not shown). To evaluate if the SN was detectable in metastatic LNs, we performed an MRI experiment using the same procedure in the metastatic rat model at 18 days after A431 cell injection as that used in the normal rat model. Clear signal reduction in the Br with a large susceptibility effect was observed after MNP injection (Fig. 7e,f). In the metastatic and normal models, M20 accumulation in the Br was higher than in the Ax. This result indicated that 20-nm MNPs were selective and can be used as an SN tracer, even in the metastatic model.

Exploratory Single Toxicity Study of 20-nm MNPs

An exploratory single toxicity study was performed to evaluate the toxicity of the MNPs. Overall animal condition and body weight status were observed (Fig. 8). All of the mice (two out of two) in the high-dose group died within 1 minute after injection, and 50% of the mice (two out of four) died in the medium-high-dose group after 3 and 15 minutes. The other two mice in the medium-high-dose group exhibited weight loss on day 1. Both mice subsequently recovered from this initial weight loss. The tolerable dose of MNPs was the medium-low dose (1250 μmol/kg) injection. This indicated that the fatal dose was almost equal to that for Ferucarbotran. Histopathological analysis revealed

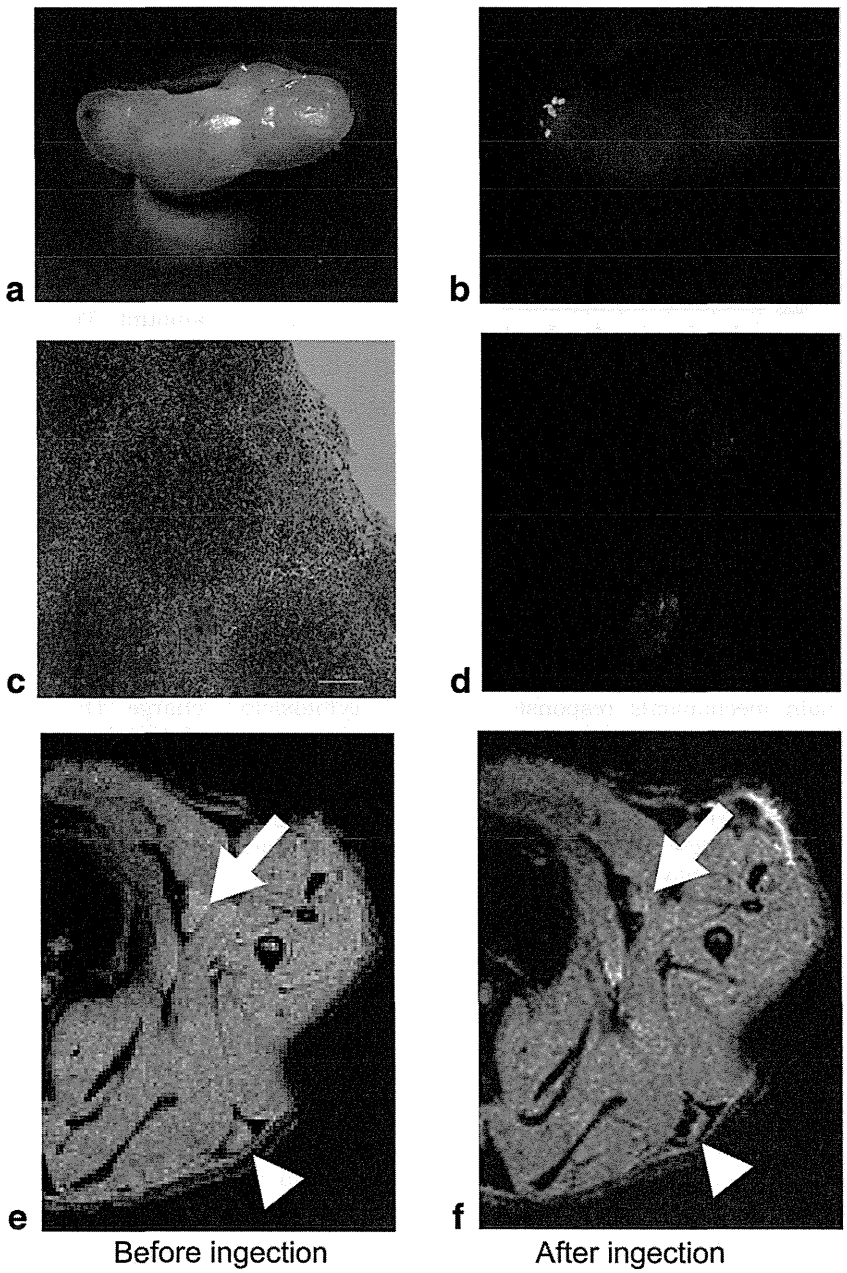

Figure 7. LN image at 18 days after A431 cell inoculation (**a**). A431 tumor transfected with green fluorescent protein (GFP) in the SN was visualized under a fluorescence stereoscopic microscope (**b**). The samples of tissue that were harvested from the Br were evaluated using H&E staining (**c**) and confirmed using a fluorescence microscope (**d**). Gradient echo images before injection (**e**) and after injection (**f**) show M20-MNPs in the tumor model. The arrowhead indicates the Br and the arrow indicates the Ax.

accumulation of MNPs in lung, liver, and spleen (Fig. 9a–r).

DISCUSSION

In the present study we demonstrated that our precisely sized 20-nm MNPs uniformly coated with citrate, used in combination with MRI, had good dispersion in solution and functioned as a specific SN detection agent, even in the case of metastatic nodes in the rodent model. The dye and radioactive tracer methods are the most widely used for identifying the SN from biopsies in cancer patients (26), but some disadvantages remain. The dye method can sometimes cause anaphylactic shock and has technical difficulties associated with SN detection. There are also technical difficulties associated with the use of the radioactive tracer method that include external γ-probe counting and radiation exposure. Radioscintigraphy is a whole-body screening technique that when used for preoperative SN screening has poor imaging spatial resolution, which limits its value for accurate identification of the detailed anatomy of the lymphatic drainage basin.

Our method using 20-nm MNPs has the potential to resolve these problems. MRI could be one of the useful methods for whole-body SN scanning, and has a number of potential advantages over radioscintigraphy. These include higher temporal resolution, higher

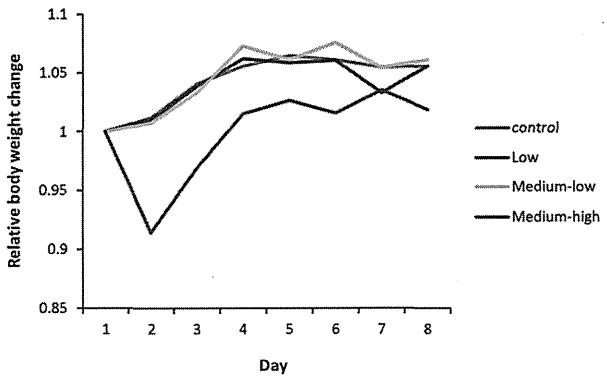

Figure 8. Weight change profile of animals after the administration of M20 MNPs into the tail vein. Control: saccharose fluid injection; Low dose: 625 μmol/kg; Medium-low dose: 1250 μmol/kg; Medium-high dose: 2500 μmol/kg; High dose: 5000 μmol/kg.

spatial resolution that enables the depiction of lymphatic channels, acquisition of 3Dimages, and the absence of radiation exposure. Generally speaking, MNPs can have potential ecytotoxic effects. One of the main mechanisms responsible for MNP cytotoxicity involves their response to reactive oxygen species (ROS); these are generated by the release of free iron ions and can lead to oxidative stress. ROS disturb the balance between oxidative pressure and antioxidant defense, which results in DNA damage (27,28). Previous studies have reported that USPIO-enhanced MRI is useful in the diagnosis of metastatic lymph nodes and that the use of this modality will be helpful in treatment decision-making for several organs (14,19–22). However, USPIO has been reported to have no specificity for the SN (29,30), and it remains difficult to identify the SN and to judge whether it has metastasis.

In contrast, our 20-nm MNPs demonstrated high selectivity for the SN, and their toxicity was the same as that of Ferucarbotran. MR lymphography with MNPs has the potential to enable us to predict the accurate anatomic location of the SN preoperatively in the clinic.

The special features of MNPs are uniform size, good dispersion in solution, and a surface coating (23). These features might influence their selective targeting of the SN. Particle size is one of the most important factors in SN identification (31). We explored the optimal size of MNPs by comparing 4-, 8-, and 20-nm MNPs with Ferucarbotran as a control, and found that 20-nm MNPs had the best diameter for SN identification. This diameter is within the range of several nm to a couple of hundred nm, as suggested by previous studies (31,32). Generally speaking, the effectiveness of the tracer draining into the lymphatic system depends on particle size. The smaller particles (diameters of less than 4–5 nm) are cleared from the injection site and exchanged through blood capillaries (33). The medium-sized particles (diameters of tens of nm) travel across the lymphatic capillaries and are trapped in the first LN (34). The larger particles (diameters of hundreds of nm) remain trapped at the injection site and can be retained for extended periods at the injection site (34). Bergqvist et al (35) found that both the total and specific uptake of particle colloids in parasternal LNs in rabbits was highest for when they had sizes between 10 and 50 nm.

Dose is another important factor in SN identification. In the present study we examined a range of doses of MNPs for SN identification using MRI. We found in the case of 20-nm MNPs, when evaluated in a rat model, that 0.4 mg/kg was the most appropriate amount. The level of 20-nm MNPs was found to be higher in the Br and lower in the Ax than the threshold value, only in the case of the 0.4 mg/kg injection dose. This was confirmed pathologically. In addition, in clinical use it is necessary to be able to detect the SN, even if micrometastasis is present. Lymphatic flow could change when metastasis exists in the LN. In our study, we established a metastatic rat model, and as was the case with our normal rat model, 20-nm MNP proved to be an ideal tracer for use with MRI.

There are other possible factors that could influence SN localization using MNPs; for example, the surface coating material and the surface electric charge. The benefit of our 20-nm MNPs is uniform size and good dispersion in solution. These are important factors in obtaining reproducible results. MNPs that are larger than 20 nm in size easily adhere to each other owing to magnetic attraction, and as a consequence good dispersion in solution is not possible (23). The surface charge on our MNPs and Ferucarbotran was approximately −40 mV. The surfaces of our MNPs are coated with citric acid, whereas the surfaces of the Ferucarbotran particles are coated with carboxydextran (23). Ferucarbotran that has an overall hydrodynamic diameter of 62 nm easily reached the distant node.

It has been reported that macrophages can influence the accumulation of SPIO in lymph nodes (18,36,37). The other characteristic feature of our MNPs is that they travel quickly (30 min) through lymphatic channels, and are retained in the SN for a significant period of time that exceeds 24 hours; however, the excretion time of the MNPs was not examined in our study.

Our 20-nm MNPs exhibited special characteristics that make them a useful SN tracer with the potential to solve the above-mentioned problems associated with the use of other tracer techniques. MRI with 20-nm MNPs as an SN tracer was confirmed as a high-resolution SN identification method that could potentially replace radioscintigraphy as a preoperative SN mapping method. In addition, our MNPs have potential as an SN tracer for intraoperative SN detection. The phenomenon known as magneto-acoustics, which involves sonic-wave emission by magnetically stimulated MNPs, was discovered in 1994 (38). We are in the process of developing a handheld device for SN detection during surgery. Using our 20-nm MNPs, we believe that in the near future we will be able to detect the SN before surgery using MRI and during surgery using our handheld device in the operating room.

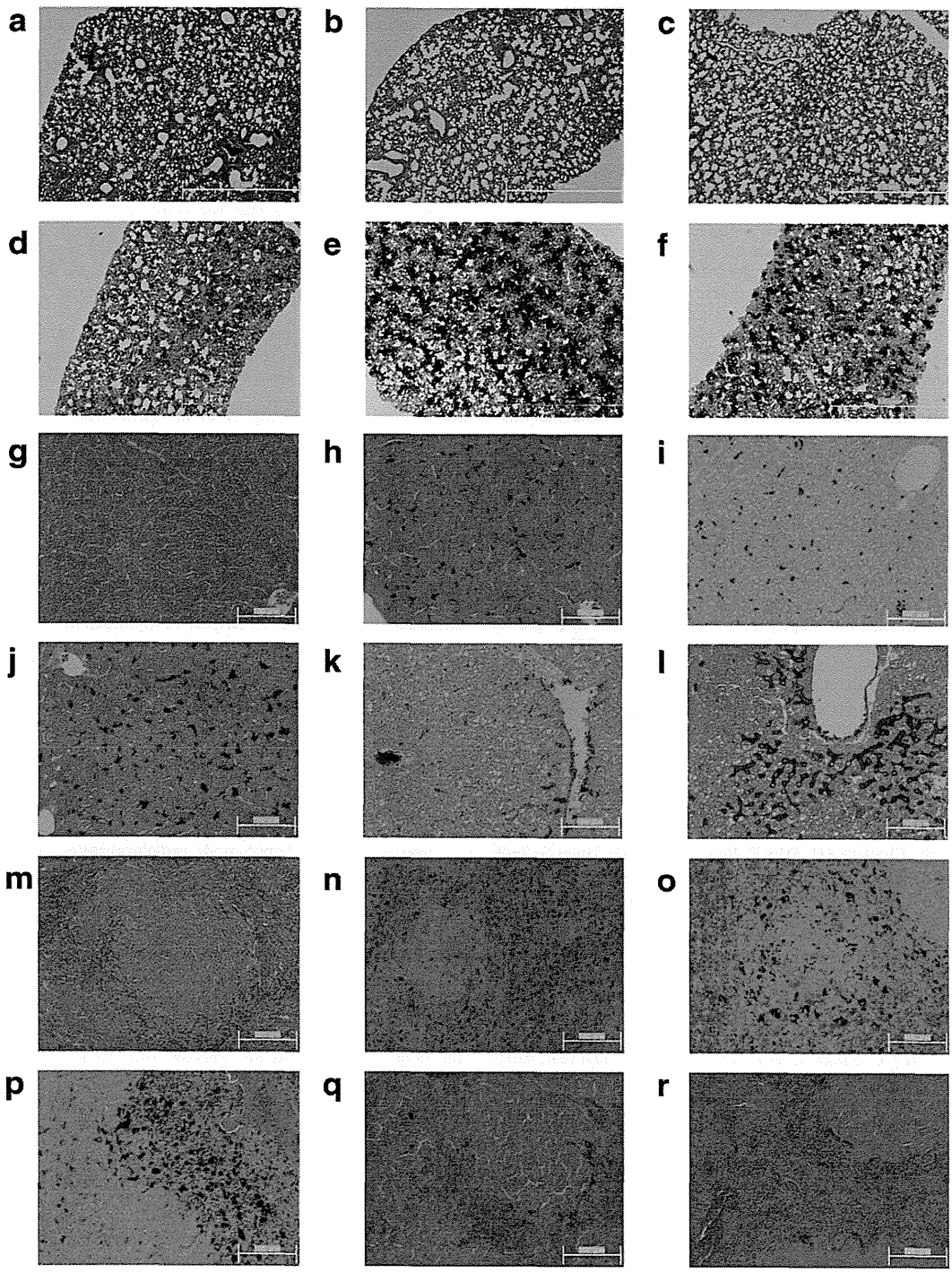

Figure 9. Prussian blue-stained tissue sections of lung/liver/spleen in the control group (**a/g/m**), in the low-dose group (**b/h/n**), in the medium-low dose group (**c/i/o**), in the medium-high-dose group (alive; **d/j/p**), in the medium-high-dose group (dead; **e/k/q**), and in the high-dose group (**f/l/r**).

In conclusion, we have developed a new MNP that is an ideal SN tracer and a useful SN identification method, using MRI with 20-nm MNPs as an SN tracer in rodent SN and SN metastasis models. This tracer could solve the problems associated with the use of other tracer techniques.

ACKNOWLEDGMENTS

The authors thank Masakazu Ueda, MD, PhD (Department of Surgery, School of Medicine, Keio University) for valuable discussion and continuing interest and encouragement, who died before the article

was completed. We thank Sayaka Shibata (NIRS) and Toshihide Muramatsu for assistance with experiments involving MRI measurements.

REFERENCES

1. Eifel P, Axelson JA, Costa J, et al. National Institutes of Health Consensus Development Conference Statement: adjuvant therapy for breast cancer, November 1–3, 2000. J Natl Cancer Inst 2001; 93:979–989.
2. Yoshino I, Nakanishi R, Osaki T, et al. Unfavorable prognosis of patients with stage II non-small cell lung cancer associated with macroscopic nodal metastases. Chest 1999;116:144–149.
3. Esser S, Reilly WT, Riley LB, Eyvazzadeh C, Arcona S. The role of sentinel lymph node mapping in staging of colon and rectal cancer. Dis Colon Rectum 2001;44:850–854; discussion 854–856.
4. Paramo JC, Summerall J, Wilson C, et al. Intraoperative sentinel lymph node mapping in patients with colon cancer. Am J Surg 2001;182:40–43.
5. Saha S, Bilchik A, Wiese D, et al. Ultrastaging of colorectal cancer by sentinel lymph node mapping technique—a multicenter trial. Ann Surg Oncol 2001;8(9 Suppl):94S–98S.
6. Kitagawa Y, Fujii H, Mukai M, et al. Intraoperative lymphatic mapping and sentinel lymph node sampling in esophageal and gastric cancer. Surg Oncol Clin N Am 2002;11:293–304.
7. Takeuchi H, Fujii H, Ando N, et al. Validation study of radioguided sentinel lymph node navigation in esophageal cancer. Ann Surg 2009;249:757–763.
8. Kitagawa Y, Kubota T, Otani Y, et al. [Clinical significance of sentinel node navigation surgery in the treatment of early gastric cancer.] Nippon Geka Gakkai Zasshi 2001;102:753–757.
9. Bergkvist L, Frisell J, Liljegren G, Celebioglu F, Damm S, Thorn M. Multicentre study of detection and false-negative rates in sentinel node biopsy for breast cancer. Br J Surg 2001;88:1644–1648.
10. Krag DN, Weaver DL, Alex JC, Fairbank JT. Surgical resection and radiolocalization of the sentinel lymph node in breast cancer using a gamma probe. Surg Oncol 1993;2:335–339; discussion 340.
11. Albertini JJ, Lyman GH, Cox C, et al. Lymphatic mapping and sentinel node biopsy in the patient with breast cancer. JAMA 1996;276:1818–1822.
12. Klausen TL, Chakera AH, Friis E, Rank F, Hesse B, Holm S. Radiation doses to staff involved in sentinel node operations for breast cancer. Clin Physiol Funct Imaging 2005;25:196–202.
13. Mertes PM, Malinovsky JM, Mouton-Faivre C, et al. Anaphylaxis to dyes during the perioperative period: reports of 14 clinical cases. J Allergy Clin Immunol 2008;122:348–352.
14. Anzai Y, Blackwell KE, Hirschowitz SL, et al. Initial clinical experience with dextran-coated superparamagnetic iron oxide for detection of lymph node metastases in patients with head and neck cancer. Radiology 1994;192:709–715.
15. Bellin MF, Roy C, Kinkel K, et al. Lymph node metastases: safety and effectiveness of MR imaging with ultrasmall superparamagnetic iron oxide particles—initial clinical experience. Radiology 1998;207:799–808.
16. Bulte JW, Kraitchman DL. Iron oxide MR contrast agents for molecular and cellular imaging. NMR Biomed 2004;17:484–499.
17. Kitamura N, Kosuda S, Araki K, et al. Comparison of animal studies between interstitial magnetic resonance lymphography and radiocolloid SPECT/CT lymphoscintigraphy in the head and neck region. Ann Nucl Med 2012;26:281–285.
18. Weissleder R, Elizondo G, Josephson L, et al. Experimental lymph node metastases: enhanced detection with MR lymphography. Radiology 1989;171:835–839.
19. Anzai Y, Prince MR. Iron oxide-enhanced MR lymphography: the evaluation of cervical lymph node metastases in head and neck cancer. J Magn Reson Imaging 1997;7:75–81.
20. Harisinghani MG, Saini S, Slater GJ, Schnall MD, Rifkin MD. MR imaging of pelvic lymph nodes in primary pelvic carcinoma with ultrasmall superparamagnetic iron oxide: preliminary observations. J Magn Reson Imaging 1997;7:161–163.
21. Nishimura H, Tanigawa N, Hiramatsu M, Tatsumi Y, Matsuki M, Narabayashi I. Preoperative esophageal cancer staging: magnetic resonance imaging of lymph node with ferumoxtran-10, an ultrasmall superparamagnetic iron oxide. J Am Coll Surg 2006;202: 604–611.
22. Tatsumi Y, Tanigawa N, Nishimura H, et al. Preoperative diagnosis of lymph node metastases in gastric cancer by magnetic resonance imaging with ferumoxtran-10. Gastric Cancer 2006;9: 120–128.
23. Hatakeyama M, Kishi H, Kita Y, et al. A two-step ligand exchange reaction generates highly water-dispersed magnetic nanoparticles for biomedical applications. J Mater Chem 2011; 21:5959–5966.
24. Park J, An K, Hwang Y, et al. Ultra-large-scale syntheses of monodisperse nanocrystals. Nat Mater 2004;3:891–895.
25. Sun S, Zeng H, Robinson DB, et al. Monodisperse MFe2O4 (M = Fe, Co, Mn) nanoparticles. J Am Chem Soc 2004;126:273–279.
26. Krag D. Minimal invasive staging for breast cancer: clinical experience with sentinel lymph node biopsy. Semin Oncol 2001;28: 229–235.
27. Ding J, Tao K, Li J, Song S, Sun K. Cell-specific cytotoxicity of dextran-stabilized magnetite nanoparticles. Colloids Surf B Biointerfaces 2010;79:184–190.
28. Lewinski N, Colvin V, Drezek R. Cytotoxicity of nanoparticles. Small 2008;4:26–49.
29. Rogers JM, Jung CW, Lewis J, Groman EV. Use of USPIO-induced magnetic susceptibility artifacts to identify sentinel lymph nodes and lymphatic drainage patterns. I. Dependence of artifact size with subcutaneous Combidex dose in rats. Magn Reson Imaging 1998;16:917–923.
30. Torchia MG, Nason R, Danzinger R, Lewis JM, Thliveris JA. Interstitial MR lymphangiography for the detection of sentinel lymph nodes. J Surg Oncol 2001;78:151–156; discussion 157.
31. Jimenez IR, Roca M, Vega E, et al. Particle sizes of colloids to be used in sentinel lymph node radiolocalization. Nucl Med Commun 2008;29:166–172.
32. Higashi H, Natsugoe S, Uenosono Y, et al. Particle size of tin and phytate colloid in sentinel node identification. J Surg Res 2004; 121:1–4.
33. Henze E, Schelbert HR, Collins JD, Najafi A, Barrio JR, Bennett LR. Lymphoscintigraphy with Tc-99m-labeled dextran. J Nucl Med 1982;23:923–929.
34. Keshtgar MR, Ell PJ. Sentinel lymph node detection and imaging. Eur J Nucl Med 1999;26:57–67.
35. Bergqvist L, Strand SE, Persson BR. Particle sizing and biokinetics of interstitial lymphoscintigraphic agents. Semin Nucl Med 1983;13:9–19.
36. Tanoura T, Bernas M, Darkazanli A, et al. MR lymphography with iron oxide compound AMI-227: studies in ferrets with filariasis. AJR Am J Roentgenol 1992;159:875–881.
37. Vassallo P, Matei C, Heston WD, McLachlan SJ, Koutcher JA, Castellino RA. Characterization of reactive versus tumor-bearing lymph nodes with interstitial magnetic resonance lymphography in an animal model. Invest Radiol 1995;30:706–711.
38. Roth BJ, Basser PJ, Wikswo JP Jr. A theoretical model for magneto-acoustic imaging of bioelectric currents. IEEE Trans Biomed Eng 1994;41:723–728.